Available online at www.sciencedirect.com
SCIENCE DIRECT®
Intermetallics 12 (2004) 945–950
Intermetallics
www.elsevier.com/locate/intermet

Effects of environment and temperature on the mechanical behavior of the Ni–19Si–3Nb intermetallic alloy doped with boron and carbon

Jason S.C. Jang[a,*], H.R. Wong[a], L.J. Chang[a], S.J. Wong[b]

[a]*Department of Materials and Engineering, I-Shou University, 1 Sec.1, Shiuecheng Road, Kaohsiung, Taiwan ROC*
[b]*Materials Research Laboratories, ITRI, Taiwan, Taiwan ROC*

Available online 30 April 2004

Abstract

The effect of small additions of boron and carbon on the environment embrittlement at different temperature of Ni–19Si–3Nb based alloy was investigated by atmosphere-controlled tensile test in various conditions. The results revealed that the Ni–19Si–3Nb base alloy exhibits ductile mechanical behavior (UTS ~ 1250 MPa, $\varepsilon \sim 14\%$) at room temperature in vacuum (2×10^{-4} torr) as well as in pure oxygen atmosphere. This indicates that environmental embrittlement due to water vapor is the major factor to the deterioration of the ductility of Ni–19Si–3Nb base alloy. In parallel, 300 ppm boron addition significantly improves the ultimate tensile strength and the ductility (UTS $\geq$ 1200 MPa, $\varepsilon \geq 12\%$) in the Ni–19Si–3Nb base alloy at room temperature in various atmosphere of pure oxygen, air (contains 14000 ppm water vapor), and pure water vapor (contains 850 ppm water vapor). In addition, the yield strength of the Ni–19Si–3Nb–0.15B–0.1C alloy increases with temperature, and the maximum yield strength occurs at 873 K. However, the ductility of the Ni–19Si–3Nb–0.15B–0.1C alloy drops significantly when the temperature increases to 973 K.

Keywords: A. Intermetallics, miscellaneous; A. Sillcides, various; B. Microalloying; B. Environmental embrittlement; B. Mechanical properties at high temperatures

1. Introduction

Intermetallic compounds based on Ni_3Si are potential of using as high-temperature structural materials because Ni_3Si, like Ni_3Al, exhibits a number of interesting properties for structural applications in harsh environments at elevated temperatures [1–3]. These properties include good corrosion resistance, reasonable room-temperature (RT) ductility, and yield strength increasing with temperature. However, similar to Ni_3Al [4], binary Ni_3Si suffers from environmental embrittlement at room temperature, which is exacerbated by the presence of hydrogen. Increasing the nickel content and the addition of titanium are reported to improve the room temperature ductility of the Ni_3Si-based alloys [5–7]. In addition, the addition of Nb is also reported to improve the room temperature ductility and strength of Ni_3Si based alloys [8–10]. To further improve the mechanical and related properties of the Ni_3Si based alloy, microalloying has been attempted with small amount of interstitial elements such as boron, carbon, and beryllium, resulting in significant improvements in mechanical properties such as RT ductility [11–16]. However, these Ni_3Si-based alloys have been reported to suffer from environmental embrittlement at elevated temperatures [6,11,12,17–20]. The present study was performed to develop a further understanding of the effect of boron and carbon additions on environmental embrittlement of the Ni–19Si–3Nb–0.15B–0.1C alloy over a range of temperatures in different environments including air, vacuum, dry oxygen, and pure water vapor.

2. Experimental

Ni_3Si based alloys with the composition of Ni-19 at% Si-3 at% Nb and Ni-19 at% Si-3 at% Nb-0.15 at% B-0.1 at% C were prepared by arc-melting of the appropriate amounts of carbonyl nickel, electronic grade silicon, 99.9% pure niobium, and 99.9% pure silicon carbide, then drop-casting into a cold copper mold. The weight loss of the alloy during melting was little (the composition loss ratio of elements was less than 0.02 wt% determined by glowing discharge spectrum analysis). The ingots after annealing at 1080 °C for 4 h and aging at 700 °C for 10 h, the ingots were then machined into the tensile specimens with a gauge section of

* Corresponding author.
E-mail address: scjang@isu.edu.tw (J.S.C. Jang).

0966-9795/$ - see front matter © 2004 Elsevier Ltd. All rights reserved.
doi:10.1016/j.intermet.2004.02.024

3 mm W × 2 mm T × 20 mm L by electro-discharge machining. The sample specimen was then carefully polished to remove the damage surface layer. Tensile testing was performed at temperatures ranging from RT to 800 °C at a constant crosshead speed with an engineering strain rate of $5 \times 10^{-4}\ s^{-1}$. The tests were performed in air (with humidity around 60%), vacuum ($\sim 2 \times 10^{-4}$ torr), dry oxygen (~ 10 torr), and water vapor (~ 50 torr) environments. For those tests performed in oxygen and water vapor, a vacuum ($\sim 2 \times 10^{-4}$ torr) was achieved in the testing chamber prior to backfilling with oxygen or distilled water.

The microstructure for each alloy and the fractured surface of the specimens were both examined using a Hitachi canning electron microscope, model S-2700, operated at 15 kV and with energy dispersive spectrometer capability. In addition, samples for observation of the polished surface were metallographically prepared and etched with Marble's etching solution (HCl 50 ml + $CuSO_4$ 10 g + H_2O 50 ml). Thin foil specimens for transmission electron microscope (TEM) observation were prepared electrochemically in a solution of 10 vol.% perchloric acids and 90 vol.% methanol using a digital Fischione twin-jet electro polisher, model 110, operating at a potential of 30–40 V at −30 °C. TEM observations were performed with a JOEL CX-300 TEM operating at 300 kV. The analyses of boron and carbon segregation were examined by Auger electron spectroscopy (AES) in a Fison Microlab 310-D scanning Auger microprobe.

3. Results

3.1. Microstructures

The SEM image in Fig. 1-a shows the heat-treated microstructure of Ni–19Si–3Nb base alloy, which consists dendrite of β phase ($L1_2$ Ni_3Si), α (fcc solid solution)-β eutectic and many plate-like network precipitates existing in the β matrix. Those plate-like precipitates change to small equiaxed precipitates for the Ni–19Si–3Nb–0.15B–0.1C alloy, as shown in Fig. 1b. Figs. 2 and 3 are TEM images and the selected area diffraction (SAD) patterns obtained from thin foil of Ni–19Si–3Nb and Ni–19Si–3Nb–0.15B–0.1C alloys, respectively. These results revealed similar patterns for the continuous β phase (Ni_3Si) as well as cuboid β phase; they were characteristic of ordered fcc structure with lattice constant, a_0, of 0.3562 and 0.3714 nm, respectively, as listed in Table 1 (calculated from the measurements of SAD). Additions of boron and carbon seem to expand the lattice constant of the β phase in the Ni–19Si–3Nb–0.15B–0.1C alloy. SAD measurements for the Ni–19Si–3Nb and Ni–19Si–3Nb–0.15B–0.1C alloys, shown in Figs. 2 and 3, also resolved one structure only for the Nb-rich precipitate. The Nb-rich precipitates embedded in the β phase were characterized to be the Nb_3Ni_2Si phase with cubic structure and lattice constant of 1.153 and 1.176 nm, respectively.

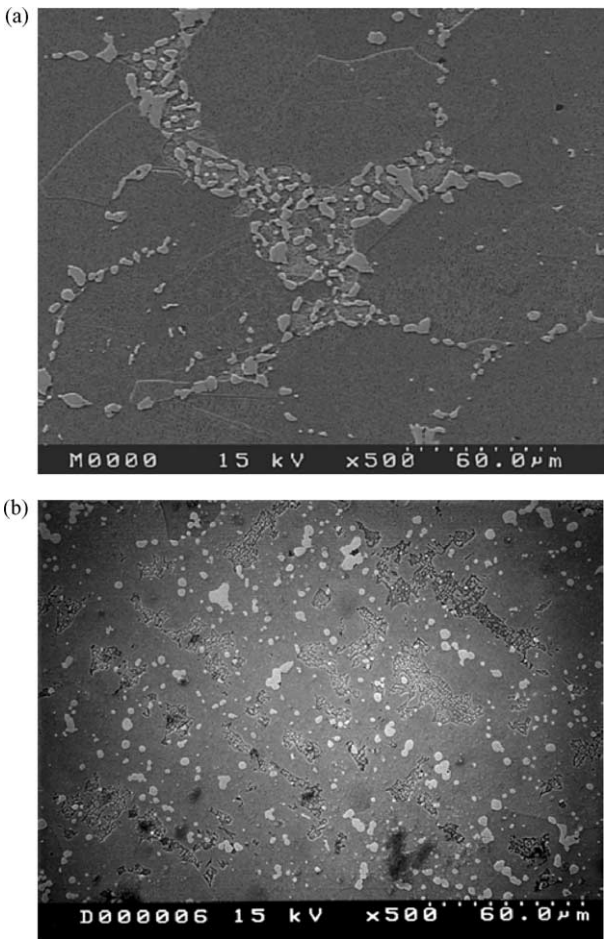

Fig. 1. The SEM metallographs of the Ni–19Si–3Nb alloy and Ni–19Si–3Nb–0.15B–0.1C alloy.

This finding is similar to the report of Jang et al. [9,14–16]. Therefore, boron and carbon additions expand the lattice of the matrix as well as the Nb_3Ni_2Si phase.

AES results shown in Fig. 4(a)–(c) reveal that boron and carbon atoms segregate to the grain boundary as well as in the Nb_3Ni_2Si precipitates. The concentration of boron and carbon is about 4.2 at% and 1.3 at% on the grain boundary, respectively, and 3.1 at% and 2.1 at% on the precipitate for the Ni–19Si–3Nb–0.15B–0.1C alloy. This measurement is similar to the results reported by Liu et al. [13] and Heatherly et al. [18]. They found that boron atoms segregate to the grain boundaries of the Ni_3Si phase and increase their cohesion, thereby changing the fracture mode from intergranular to transgranular fracture. Subramanian et al. [21] suggested that the boron elements could lower the surface energy of the $L1_2$ phase. It is suggested accordingly that boron segregation to the interface between Nb_3Ni_2Si precipitates and the β phase, thus reduce the surface energy of the precipitate. This may explain the morphology change of Nb_3Ni_2Si precipitates after microalloying with boron in the Ni–19Si–3Nb based alloys.

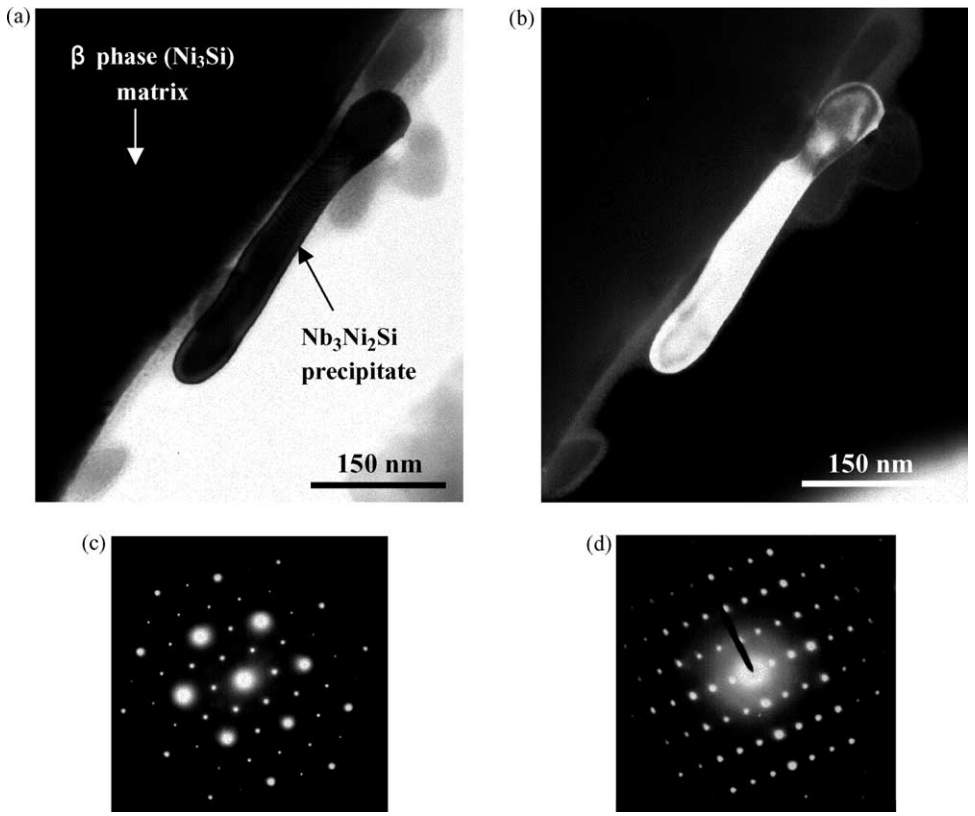

Fig. 2. TEM images and electron diffraction patterns for Ni–19Si–3Nb alloy; (a) bright field image of the matrix with precipitate, (b) dark field image from the $(\bar{3}30)$ reflection of Nb_3Ni_2Si precipitate, (c) B[111] SAD pattern ofβphase (Ni_3Si), and (c) B$[01\bar{1}]$ SAD pattern of the precipitate.

3.2. Effects of temperature on the tensile properties

Fig. 5 shows plots for the yield stress (defined at 0.2%-offset strain) of the Ni–19Si–3Nb base alloy with and without boron and carbon additions as a function of temperature. The yield stress vs. temperature curve for the Ni–19Si–3Nb base alloy as well as the Ni–19Si–3Nb–0.15B–0.1C alloy were similar. Both curves show that

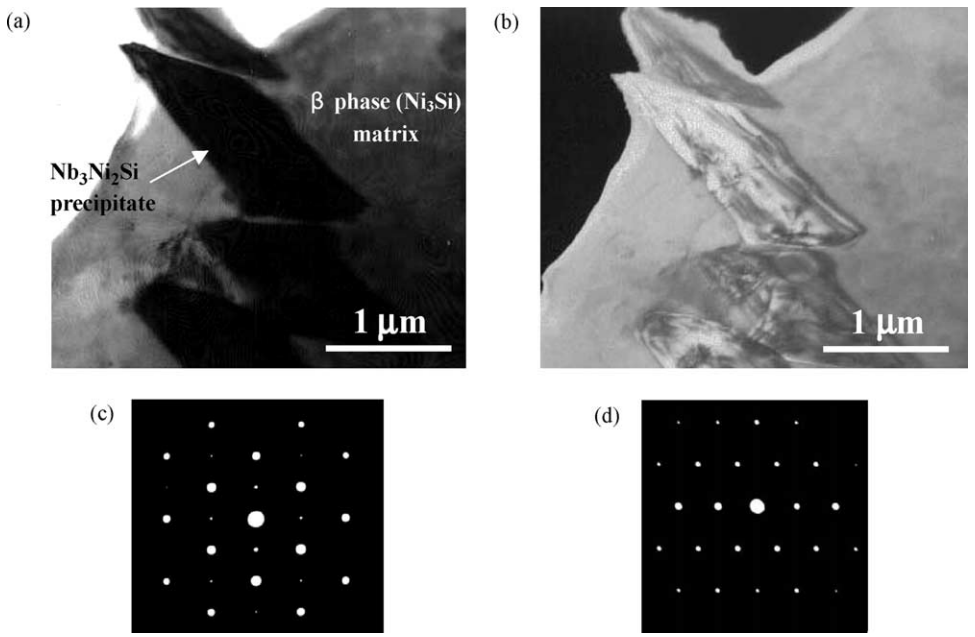

Fig. 3. TEM images and electron diffraction patterns for Ni–19Si–3Nb–0.15B–0.1C alloy; (a) bright field image of βphase (Ni_3Si) with Nb_3Ni_2Si precipitate, (b) dark field image from the (220) reflection of Nb_3Ni_2Si precipitate, (c) B$[01\bar{1}]$ SAD pattern of β phase (Ni_3Si), and (d) B$[\bar{1}13]$ SAD pattern of the precipitate.

Table 1
Lattice constant measured by SAD for the Ni–19Si–3Nb alloys with different boron and carbon content

Lattice constant	Matrix (nm)	Precipitate (nm)
Alloy		
Ni–19Si–3Nb	0.3562	1.153
Ni–19Si–3Nb–0.15B–0.1C	0.3714	1.176

the yield stress increases with temperature starting from room temperature at first, then reaches a maximum at 873 K and finally decreases rapidly as further increase in temperature. In addition, the yield stress was enhanced by the addition of boron and carbon over a wide range of temperature.

The tensile elongation of the Ni–19Si–3Nb alloy and the Ni–19Si–3Nb–0.15B–0.1C alloy as a function of temperature under different environments is shown in Fig. 6. When tested in vacuum, both Ni–19Si–3Nb alloy and Ni–19Si–3Nb–0.15B–0.1C alloy exhibited identical high elongation values (i.e. $\varepsilon > 12\%$) at room temperature. Additionally, the tensile elongation of Ni–19Si–3Nb–0.15B–0.1C alloy increases along with temperature up to 873 K, and then decreases with temperature up to 1073 K. When tensile tested in air and water vapor atmosphere, the tensile elongation of the unalloyed Ni–19Si–3Nb exhibited relatively low values from room temperature ($\sim 5\%$) to 1073 K ($< 2\%$). With additions of 0.15 at% B and 0.1 at% C, the tensile elongation was significantly improved over a wide range of temperature under both air and 50 torr water vapor atmospheres.

The ultimate tensile strength (UTS) of the Ni–19Si–3Nb alloy and Ni–19Si–3Nb–0.15B–0.1C alloy as a function of temperature is shown in Fig. 7. Both alloys attain high values of UTS (i.e. > 1200 MPa) at room temperature when tested in vacuum. In addition, the tensile strength in vacuum of these two alloys increases with temperature up to 873 K, and then decreases with temperature from 873–1073 K. When tested in air and pure water vapor, the Ni–19Si–3Nb–0.15B–0.1C alloy displays higher UTS values than the Ni–19Si–3Nb alloy over the entire temperature range. The results of UTS appear to be well correlated with those results of tensile elongation.

4. Discussion

It has been suggested that the environmental effect at low temperatures is associated with hydrogen-induced embrittlement [22–24]. While at high temperature, the environmental effect is related with oxygen-induced embrittlement [8,25]. Therefore, the effect of boron addition on the suppression of environmental embrittlement could be due to the interaction between hydrogen and boron, and the interaction between oxygen and boron in the corresponding temperature regime.

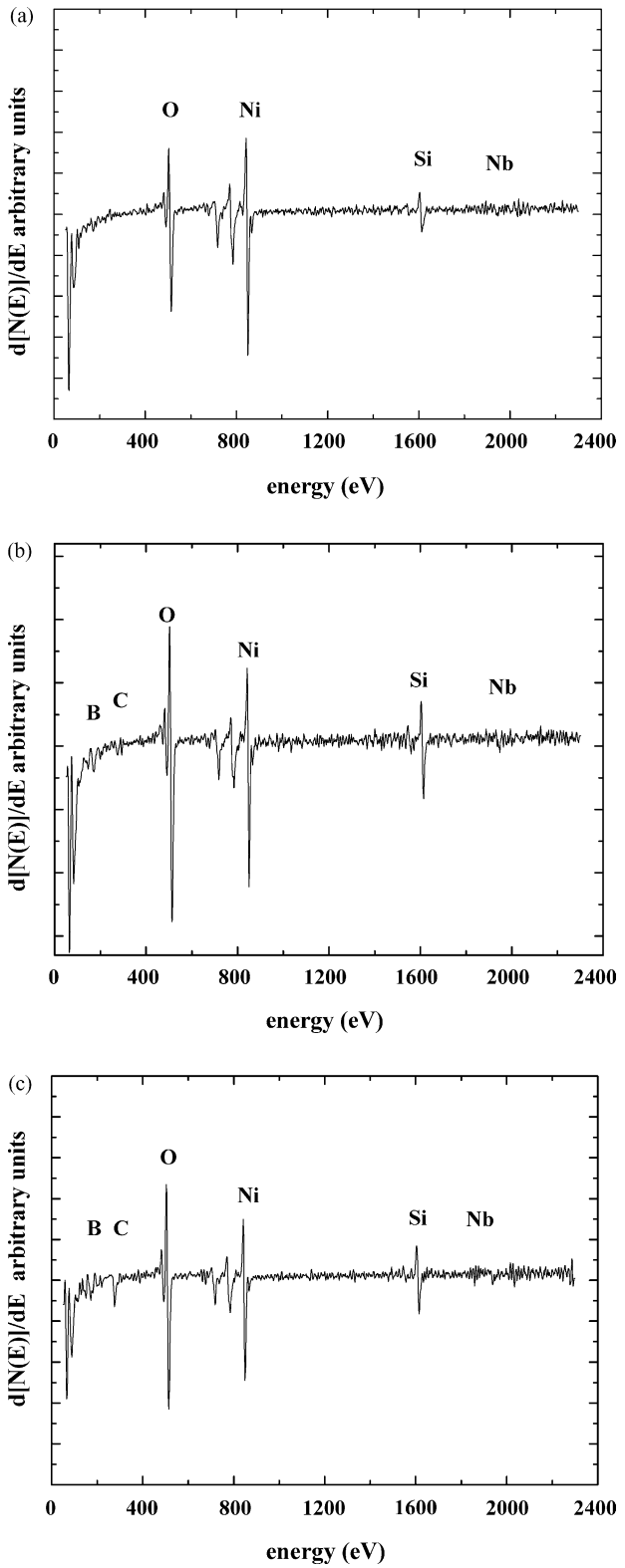

Fig. 4. Auger analyses on the selected area of Ni–19Si–3Nb–0.15B–0.1C alloy; (a) matrix, (b) grain boundary, and (c) precipitate.

The undoped Ni–19Si–3Nb alloy actually suffered from environmental (i.e. air or 850 ppm water vapor) embrittlement. This kind of environmental effect has been widely

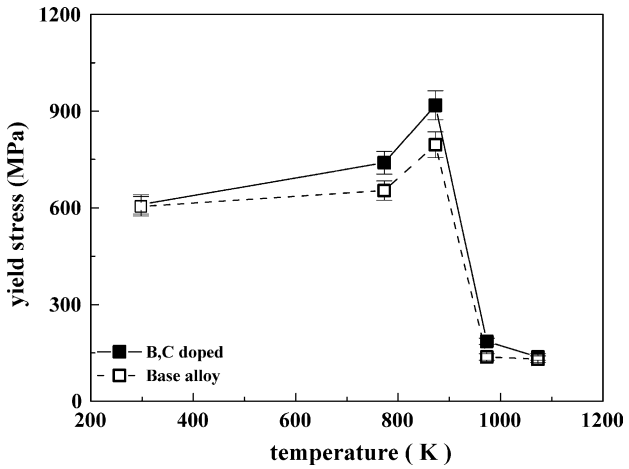

Fig. 5. Yield stress as a function of temperature for the Ni–19Si–3Nb alloy (with mark of □) and Ni–19Si–3Nb–0.15B–0.1C alloy (with mark of ■) tested in vacuum.

observed for a number of $L1_2$-type compounds [26–29]. It is recognized that environmental embrittlement in materials resulting in the fracture of materials involves kinetic process, such as decomposition, permeation and condensation of hydrogen species, and bond breaking processes [30–33]. With regard to the decomposition process of hydrogen, it has been proposed that materials deformed in air are embrittled due to atomic hydrogen decomposed from moisture (i.e. H_2O molecules). In addition, the active element (such as Si in this alloy) has been suggested to react with the moisture in air by the reaction, $Si + 2H_2O \rightarrow SiO_2 + 4H$. The generated atomic hydrogen can therefore penetrate into grain boundaries at crack tips to cause the brittle intergranular fracture. However, the results observed in the boron and carbon doped Ni–19Si–3Nb alloy clearly

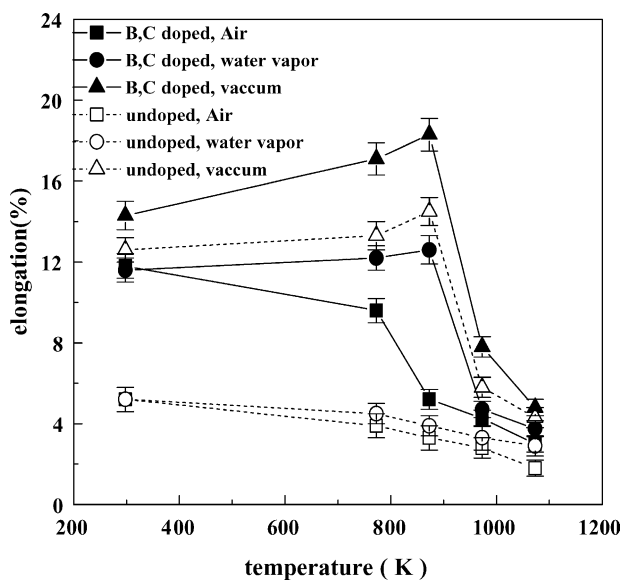

Fig. 6. Tensile elongation as a function of temperature for the Ni–19Si–3Nb alloy (with mark of □, ○,and △) and Ni–19Si–3Nb–0.15B–0.1C alloy (with mark of ■, ●,and ▲) tested in different atmosphere.

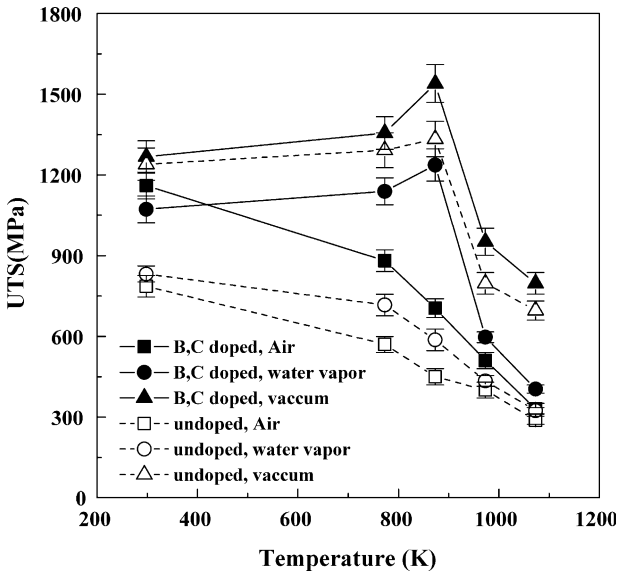

Fig. 7. Ultimate tensile strength as a function of temperature for the Ni–19Si–3Nb alloy (with mark of □, ○,and △) and Ni–19Si–3Nb–0.15B–0.1C alloy (with mark of ■, ●,and ▲) tested in different atmosphere.

indicated that boron atoms suppressed the environmental embrittlement in air and water vapor atmosphere at temperatures below 773 K, as shown in Figs. 6 and 7. Wang and Chung [34] have proposed that the strong B–H bonding may slow the hydrogen diffusion rate into the boron-doped $Ni_3(Al, Ti)$ (110) single crystal. This leads to a lower concentration of atomic hydrogen at the crack tip, thus can suppress hydrogen-induced embrittlement.

When tested in air, as the test temperature increases to the intermediate high temperature (i.e. above 873 K), the ductility of the Ni–19Si–3Nb–0.15B–0.1C alloy decreases significantly from 10 to 5.5%, as shown in Fig. 6. However, this feature is not evident in the Ni–19Si–3Nb–0.15B–0.1C alloy that tested in vacuum and in water vapor atmosphere. This result is similar to those obtained in the boron-doped Ni_3Al alloys [25] and the boron-doped $Ni_3(Si, Ti)$ alloys [12]. The loss in ductility at high temperatures (~873 K) was accompanied by a change in fracture mode from transgranular to intergranular.

5. Conclusion

The tensile properties of Ni–19Si–3Nb alloy and Ni–19Si–3Nb–0.15B–0.1C alloy were evaluated over a wide range of temperatures and different testing environments. The results of this study are summarized below:

(1) Addition of boron and carbon results in expansion of the lattice constant in the β matrix and the Nb_3Ni_2Si precipitate. This observation suggested that the additions of carbon and boron in the Ni–19Si–3Nb based alloy affect their hardness on the matrix

and precipitate but remain the same structure in β phase and Nb_3Ni_2Si precipitate.

(2) Boron and carbon addition results in improvement in tensile elongation of the Ni–19Si–3Nb based alloys over a wide range of temperature under air and water vapor atmosphere. In addition, UTS values of these alloys appear to be well correlated with those of tensile elongation.

(3) Additions of 0.15 at% boron and 0.1 at% carbon to the Ni–19Si–3Nb alloy results in complete suppression of moisture embrittlement in air and water vapor over a wide range of temperatures (room temperature to 773 K). However, the boron and carbon doped alloy still suffers from embrittlement associated with oxygen at medium high temperature (i.e. 873 K).

(4) The beneficial effect of boron and carbon addition on the environmental embrittlement of Ni–19Si–3Nb alloys is correlated with boron (or carbon) segregation to grain boundaries.

Acknowledgements

This research was sponsored by the National Science Council of the Republic of China, under the project number NSC90-2216-E-214-017. The authors are also very grateful for the assistance of TEM studies by Ms Liang-Chu Wang.

References

[1] Davis RG, Stoloff NS. Trans TMS-AIME 1965;233:714.
[2] Kumar KS. In: Westbrook JH, Fleischer RL, editors. Intermetallic compounds—principle and practice, vol. 2. Chichester, UK: Wiley; 1995. p. 211–35.
[3] Evans TE, Hart AC. Electrochem Acta 1971;16:1955.
[4] Grala EM. Mechanical properties of intermetallic compounds. New York: Wiley; 1960. p. 358.
[5] Takasugi T, Shindo D, Izumi O, Hirabayashi M. Acta Metall 1990;38: 739.
[6] Takasugi T, Nagashima M, Izumi O. Acta Metall 1990;38:747.
[7] Baker I, Yuan J, Schulson EM. Metall Trans A 1993;24A:283.
[8] Oliver WC. In: Liu CT, et al., editors. High temperature ordered intermetallic alloys III. MRS Symposium Proceeding, Pittsburgh, PA, 133.; 1989. p. 387–402.
[9] Jang JSC, Tsau CH. Mater Sci Eng 1992;A153:525.
[10] Takasugi T. J Intermetallics 2000;8:575.
[11] Takasugi T, Izumi O, Yoshida M. J Mater Sci 1991;26:1173.
[12] Takasugi T, Suenaga H, Izumi O. J Mater Sci 1991;26:1179.
[13] Liu CT, George EP, Oliver WC. J Intermetallics 1996;4:77.
[14] Jang JSC, Wong SK, Lee PY. Mater Sci Eng 2000;A281:17.
[15] Jang JSC, Cheng CY, Wong SK. Mater Chem Phys 2001;72:66.
[16] Jang JSC, Ou CJ, Cheng CY. Mater Sci Eng 2002;A239–331C:453.
[17] Takasugi T, Ma CL, Hanada S. Mater Sci Eng 1995;A192/193:407.
[18] Heatherly L, George EP, Liu CT, Kumar KS. Mater Sci Eng 1998; A245:80.
[19] Pike LM, Liu CT. Scripta Mater 2000;42:265.
[20] Varin RA, Song YK. J Intermetallics 2001;9:647.
[21] Subramanian S, Muller DA, Silcox J, Sass SL. Mater Sci Eng 1997; A239-240:297.
[22] Liu CT. In: Stoloff NS, Koch CC, Liu CT, Izumi O, editors. High-temperature order intermetallic alloys II. MRS Symposium, Pittsburgh, 81.; 1986. p. 355–67.
[23] Izumi O, Takasugi T. J Mater Res 1988;3:426.
[24] Stoloff NS. J Metals 1988;40(12):18.
[25] Liu CT, White CL. Acta Metall 1987;35:643.
[26] Liu CT, Mckamey CG, Lee EH. Scripta Metall 1990;24:385.
[27] Liu CT, George EP. Scripta Metall 1990;24:1285.
[28] George EP, Liu CT, Lin H, Pope DP. Mater Sci Eng A 1995;192(193): 277.
[29] Takasugi T, Izumi O. Acta Metall 1986;34:607.
[30] Liu CT. In: Liu CT, et al., editors. Ordered intermetallics-physical metallurgy and mechanical behavior. New York: Kluwer Academic Publishers; 1992. p. 321. p. 321.
[31] George EP, Liu. In: Nathal MV, et al., editors. Structural intermetallics 1997. Warrendale, USA: TMS; 1997. p. 693–702.
[32] Liu CT, Lee EH, Mckamey CG. Scripta Metall 1989;23:875.
[33] Stoloff NS, Liu CT. J Intermetallics 1994;2:75.
[34] Wang J, Chung YW. J Intermetallics 2001;9:349.